Journal of Molecular Liquids 348 (2022) 118401

Contents lists available at ScienceDirect

Journal of Molecular Liquids

journal homepage: www.elsevier.com/locate/molliq

ZnO nanoparticles coated with oleic acid as additives for a polyalphaolefin lubricant

Fátima Mariño [a], Enriqueta R. López [a], Ángela Arnosa [b], Manuel A. González Gómez [b], Yolanda Piñeiro [b], José Rivas [b], Carmen Alvarez-Lorenzo [c], Josefa Fernández [a,*]

[a] Laboratory of Thermophysical and Tribological Properties, Nafomat Group, Department of Applied Physics, Faculty of Physics and Institute of Materials (iMATUS), Universidade de Santiago de Compostela, 15782 Santiago de Compostela, Spain
[b] NANOMAG Laboratory, Department of Applied Physics, Faculty of Physics and Institute of Materials (iMATUS), Universidade de Santiago de Compostela, 15782 Santiago de Compostela, Spain
[c] Departamento de Farmacología, Farmacia y Tecnología Farmacéutica, I+D Farma Group (GI-1645), Facultad de Farmacia, Instituto de Materiales (iMATUS) and Health Research Institute of Santiago de Compostela (IDIS), Universidade de Santiago de Compostela, 15782 Santiago de Compostela, Spain

ARTICLE INFO

Article history:
Received 16 September 2021
Revised 16 December 2021
Accepted 23 December 2021
Available online 29 December 2021

Keywords:
Zinc oxide nanoparticles
Nanoparticle surface modification
Oleic acid coating
Nanolubricant
Tribological properties
Lubricant additives

ABSTRACT

In this work, ZnO nanoparticles (NPs) were successfully synthesized and coated with oleic acid (OA). The mean diameter of these NPs (ZnO-OA) was around 11.5 nm, their core was characterized by XRD and their coating by FTIR and Raman. Homogeneous dispersions at different concentrations (0.10, 0.25, 0.50, 0.75 and 1.00 wt%) of ZnO-OA in polyalphaolefin 40 (PAO40) oil were thermophysically and tribologically characterized. Both density and viscosity values increased with the concentration of NPs, reaching relative increments of 0.5% and 4.0%, respectively, for the 1 wt% nanodispersion. Tribological tests were performed at 353.15 K using an Anton Paar MCR 302 rheometer equipped with a tribological ball-on three-pins configuration testing module. Regarding the tribological behavior, the optimal concentration was 0.25 wt% of ZnO-OA (25% of reduction in the friction coefficient and 82% wear reduction in terms of cross sectional area, respect to those obtained with the neat base oil). The rolling mechanism owing to the spherical shape of the nanoadditives, transforming sliding friction into rolling friction, and the mending effect could explain the better tribological performance of nanolubricants with respect to that of neat PAO40. In addition, the presence of PAO40, ZnO-OA NPs and iron oxides was evidenced from confocal Raman microscopy on the worn surfaces obtained from tribological test with PAO40 + 0.25 wt% ZnO-OA dispersion.

1. Introduction

One of the critical challenges in science, technology and economy is planning long-term resource consumption and societal trend and trying to balance them in the best possible way [1]. Under the economic point of view, Holmberg and Erdemir [2] estimated that the total annual losses caused in tribological contacts in more than 2,500,000 million euros, of which 73% are attributable to friction and 27% owing to wear. Both losses can be substantially diminished utilizing new tribological solutions. Thus, the increasing demand for these new solutions in vehicles and machinery worldwide is directly related to the total energy losses to overcome friction (20%) and wear (3%). The use of novel lubricants and materials could lead to a reduction in energy losses of 40% in 15 years, saving energy up to 25% in transportation and 20% in power generation. At the same time, this energy savings may reduce global CO_2 emissions in 3,140 $MtCO_2$ [3].

Therefore, there is a growing need for high-performance lubricants, such as synthetic, semi-synthetic, and bio-based ones. Compared to mineral-based oils, synthetic base oils have better lubricity and both thermal and oxidative stabilities, properties that promote major durability. For these reasons, synthetic base oils are widely accepted [4]. The most common group of base oils among the synthetic base oils are polyalphaolefins (PAOs), which are paraffin-like liquid hydrocarbons synthesized by 1-decene polymerization followed by a hydrogenation step. PAOs present an exceptional combination of excellent properties such as high-temperature viscosity retention, shear stability, and very high oxidation-resistance potential, having a low volatility and a very low pour point [5]. In this work, polyalphaolefin 40 (PAO40) has been selected as base oil. Technical applications for PAO40 include

* Corresponding author.
E-mail address: josefa.fernandez@usc.es (J. Fernández).

https://doi.org/10.1016/j.molliq.2021.118401
0167-7322/

industrial gear and turbine oils, bearing lubricants, transmission fluids, compressor oils, or hydraulic oils.

In parallel, in recent decades, the search for new additives that are less harmful for the environment than the traditional ones that contain sulfur, chlorine or phosphorus, prompted the development of nanoparticles (NPs) as lubricants additives [6]. The nanolubricants obtained have shown great anti-friction and anti-wear effects, which depend on compositions, morphologies and sizes of the NPs [7-9]. The nanomaterials may contribute to the lubrication through several mechanisms such as rolling, mending, polishing or tribofilm formation [6].

Comparative studies have shown that metal oxide NPs, among them ZnO nanoparticles (ZnO NPs), when used as additives, improve the lubricating properties of the base oils [10,11]. In addition to their good tribological properties, ZnO NPs have other interesting properties such as large surface area–to-weight ratio, strong adsorption and high diffusion, among others [12]. Furthermore, these NPs are friendly to the environment, being free of sulfur and phosphorus.

Nevertheless, the aggregation of NPs could increase friction acting as debris due to the increase in size, so the dispersibility of NPs in the oils is a concern to be solved. There are two main approaches to facilitate NP dispersion in the oil and to prevent aggregation. One strategy is the incorporation of dispersants, and the other is the chemical modification of the NPs surface with an organic coating. According to Chen et al. [13], without a suitable dispersion method, aggregation always occurs, regardless of the nature or the shape of the NPs. One of the best methods to increase the stability time of the dispersions is to bind surfactant molecules on the NPs surface. Thus, it has been pointed out that functionalization with surfactants is adequate for NPs with size smaller than 50 nm, and the best stability results have been reported for NPs of 10 nm or less due to steric stabilization [13].

Regarding the first strategy and ZnO NPs, Hernández Battez et al. [14] analyzed the tribological behavior of uncoated ZnO NPs (20 nm) as additives of a polyalphaolefin (PAO6) with two non-ionic commercial dispersants (OL100 and a poly-12-hydroxy stearic acid) using four-ball test, showing good results in extreme pressure conditions. Nevertheless, the stability of NP dispersions containing the dispersants was still poor, especially for OL100. Gara and Zou [15] used oleic acid (OA) to disperse ZnO NPs (diameter 40–100 nm) into a paraffinic mineral oil, claiming improvements in the stability of the dispersions in comparison with those without OA. In addition, these authors show that oleic acid as a dispersant reduces friction coefficient to some extent. With respect to the second general strategy, Ran et al. [52] dispersed OA surface-modified ZnO NPs (core diameter 10–30 nm) in a mineral oil (60SN base oil) obtaining a stability of 12 h for concentrations up to 0.5 wt% and reductions around 29% and 15% for friction coefficients and wear scar diameter, respectively, in comparison to the base oil. Wu et al. [12] modified ZnO NPs with OA and tested them as lubricant additives in a PAO, likely a mixture of PAO2, PAO3 and PAO4, and in diisooctyl sebacate, claiming that the coating of the ZnO NPs with OA significantly improved their dispersibility in both oils. In addition, tribological performance of OA-modified ZnO (4.04 nm) as additives in PAO (optimal concentration in NPs 1.2 wt%) was better than in sebacate, with reductions of up to 9.9% for the friction coefficient and up to 31.2% for the wear scar diameter compared to those of neat PAO.

Overall, there is still a paucity of information on the use of ZnO coated NPs as friction modifiers, and further quantitative research of the stability and tribological performance of their dispersions in other base oils is required. Thus, one of the aims of this work was to obtain homogeneous dispersions at different concentrations of ZnO NPs coated with oleic acid, ZnO-OA, in PAO40. For this purpose, visual control of the dispersions as well as refractive index measurements were carried out. In order to obtain nanolubricants with long stabilities, after synthesis the NPs were dispersed by the evaporation method [17] which consists of storing the NPs in a volatile solvent, in this case chloroform. Subsequently, this dispersion is added to the oil and the chloroform is removed by means of a rotary evaporator, obtaining a dispersion of the NPs in the oil. In addition, in this work the tribological performance of the designed nanolubricants was evaluated. Thus, tribological tests were performed at 353.15 K using an Anton Paar MCR 302 rheometer equipped with a tribological ball-on-three pins module. The temperature value was chosen because in the wind turbines gearboxes the oil can reach values around 353 K [18,19]. The tribological mechanisms of the dispersions were analyzed by 3D profilometry and confocal Raman microscopy on the worn tracks of the tested pins.

2. Experimental section

2.1. Synthesis and characterization of NPs

2.1.1. Materials and reagents

Polyalphaolefin PAO40 was provided by Repsol; at 313.15 K PAO40 has a density of 0.8342 g cm^{-3}, a kinematic viscosity of 398.6 cSt and a viscosity index of 151.5. PAO40 sample was previously characterized by MALDI-TOF mass, FTIR and Raman spectroscopy [20,21]. The reagents used in the synthesis of ZnO NPs were: zinc acetate dihydrate (≥98%), potassium hydroxide (≥85%) and oleic acid (90%) from Sigma-Aldrich (Saint Louis, MO, USA); acetone (reagent grade) and ammonium hydroxide (25%) from Fisher Scientific (Waltham, MA); hydrochloric acid (37%) used to neutralize the ZnO dispersion (Acros Organics, Geel, Belgium) and absolute ethanol used as the reaction solvent (Scharlab, Barcelona, Spain). All these products were used without further purification.

2.1.2. Synthesis of ZnO NPs

ZnO NPs were prepared using Shamhariet et al. [22] method through the following reaction:

$$Zn(CH_3COO)_2 \cdot 2H_2O + 2KOH \xrightarrow{60^\circ C,EtOH} ZnO + 2CH_3COOK + 2H_2O$$

Briefly, $Zn(CH_3COO)_2{\cdot}2H_2O$ (1.49 g) was dissolved in absolute ethanol (64 mL) in a Schott bottle which contains a magnetic stirring bar, the blend being heated to 60 °C. KOH (0.79 g) was dissolved separately in absolute ethanol (30 mL) under the same conditions, the solution being slowly added dropwise to the Zn $(CH_3COO)_2{\cdot}2H_2O$ solution at 60 °C. After 3 h of magnetic stirring at 500 rpm, ZnO precipitated and was collected by centrifugation (4000 rpm) for 10 min, washed twice with acetone and once with ultrapure water. Finally, ZnO was dispersed in ultrapure water for storage, the dispersion concentration being determined by thermogravimetric analysis (TGA) using a Perkin Elmer Pirys 7 TGA (Perkin, Waltham, MA, USA). The measurements were made from 50 to 850 °C at a heating rate of 10 °C/min under a nitrogen flow of 20 mL/min and have an uncertainty of 2%.

2.1.3. Oleic acid coating of ZnO NPs

The ZnO NPs were coated with OA using the following reaction:

$$ZnO + OA \xrightarrow[2)95^\circ C,\ reflux,\ 2h]{NH_4OH\ 1)60^\circ C,\ 30\,min} ZnO - OA$$

The as prepared ZnO water dispersion was sonicated for 15 min in a Fisherbrand ultrasonic bath, with an effective power of 180 W

and a sonication frequency of 37 kHz. Then, 100 mg (12.9 mL) of this dispersion were introduced in a round-bottom flask, provided with a magnetic stir bar, and heated to 60 °C. Once the setting temperature was reached, NH_4OH (2.4 mL) was added, and 1 min later OA (300 mg, 0.27 mL) was also added. The mixture was kept at 60 °C for 30 min and then the temperature was raised to 95 °C with reflux for 2 h. The excess of NH_4OH was neutralized with HCl (9 vol %) and the precipitate (ZnO-OA) was collected by centrifugation under the same conditions as ZnO NPs and washed with ultrapure water and hexane. This washing step is done to remove excess oleic acid, as well as other soluble by-products. The ZnO-OA NPs were dispersed in chloroform for storage. The concentration of this dispersion was determined also by TGA.

2.1.4. Nanoparticle characterization

The morphology of the ZnO-OA NPs was determined using a JEOL JEM-1011 transmission electron microscope (TEM) at 100 kV acceleration voltage. The number of OA molecules per surface area of each nanoparticle was determined by TGA and by TEM. Taking into account the uncertainties associated to the size distribution of TEM measurements, to the OA content (2%) and to the ZnO-OA estimated density, the uncertainty for the number of OA molecules per surface area is estimated to be 3%. The crystal structure of ZnO-OA NPs was determined by X-ray diffraction (XRD), using a Philips PW1710 diffractometer with a graphite diffracted beam monochromator and a copper radiation source (λ (Cu Kα) = 1.5406 Å), at 40 kV and 30 mA. Measurements were carried out for a 2θ angle from 10° to 80° every 0.02° and 10 s/step on the powder sample.

The analysis of the surface functional groups of the NPs was carried out using a Thermo Nicolet Nexus Fourier Transform Infrared (FTIR) spectrometer in the attenuated total reflectance mode from 4000 to 400 cm^{-1} and a confocal Raman microscope (WITec Alpha300R+) with a green laser (532 nm) as well as the WITec Project FIVE software to process the data.

2.2. Preparation of dispersions and stability analysis

Homogeneous dispersions were prepared at different concentrations of ZnO-OA in PAO40 using the dispersion method reported by Liñeira et al. [17]. Previously, several tests were carried out to find the optimal conditions of time and temperature necessary to remove completely the chloroform and transfer the NPs to PAO40 with a rotary evaporator. For this task, chloroform was mixed with PAO40 and afterwards evaporated using the rotary evaporator at different temperatures during several times. After each temperature–time test, the viscosity of the sample was measured with a rotational viscosimeter Stabinger SVM3000 (Anton Paar, Graz, Austria). The viscosity values, from 5 to 100 °C, were compared with those of neat PAO40, considering as optimal temperature–time conditions those for which viscosity values of neat PAO40 and of the sample were closest, being these conditions: 60 °C and 30 min. After that, the 1.00 wt% ZnO-OA dispersion in PAO40 was prepared using these conditions. For this purpose, the first step was to mix the appropriate amounts of PAO40 and the ZnO-OA/chloroform dispersion. Subsequently, this blend was homogenized with both the Fisherbrand ultrasonic bath at the above-indicated conditions and a Branson ultrasonic Sonifier S-250A probe sonicator for 5 min with 200 W of effective power and 60 Hz sonication frequency with a 20% amplitude followed by evaporation, as shown in Fig. 1. The obtained PAO40 + 1.00 wt % ZnO-OA dispersion was then further sonicated for 240 min using a homogenizer Fisherbrand ultrasonic bath, in a continuous shaking mode at 180 W effective power and 37 kHz sonication frequency. Two replicates were prepared, one for the stability study, and the other for thermophysical and tribological characterizations. The other dispersions (0.10, 0.25, 0.50, 0.75 wt%) were obtained by diluting the PAO + 1.00 wt% ZnO-OA nanodispersion with PAO40. All the nanodispersions were further sonicated in the Fisherbrand ultrasonic bath under the same conditions.

Two methods were used to study the stability of the nanodispersions: visual control, taking photographs of the nanolubricants over time, and the temporal evolution of their refractive indices. For this purpose, a Mettler Toledo refractometer (RA-510 M) was used to record the refractive index (n) at 298.15 K every 5 h, operating at the wavelength of the sodium D-line (589.3 nm). The refractometer works within the n range of 1.32 to 1.56 with a resolution of 0.00001 and an uncertainty of $2{\cdot}10^{-5}$ [23].

2.3. Characterization of the nanolubricants

2.3.1. Density, viscosity, and viscosity index

An Anton Paar SVM3000 rotational Stabinger viscometer was used to determine the thermophysical properties of PAO40 and the five nanolubricants, from 298.15 K to 373.15 K and 0.1 MPa. The device and experimental procedure have been previously detailed [24]. A thermostat with cascaded Peltier elements controls the temperature inside the cell, being measured with an expanded uncertainty, k = 2, of 0.02 K through a Pt100 resistance. This viscometer has a cylindrical geometry with a rapidly rotating outer tube and a slower rotating inner bob. It is based on a modified Couette principle. A glass vibrating U-tube densimeter allows the Stabinger SVM3000 to measure the density according to the standard DIN 51 757 with an expanded uncertainty of 0.0005 g cm^{-3}. The expanded uncertainty of dynamic viscosity is 1%. Viscosity index (VI) is determined with ASTM D2270 standard [25] with an estimated uncertainty of 2.7. For each sample, these thermophysical properties have been measured once due to the excellent repeatability of the device.

2.3.2. Tribological tests

Rotational tribological tests with PAO40 and the nanodispersions were carried out with an MCR 302 modular rheometer from Anton Paar equipped with a Peltier heated T-PTD200 tribological module operating in the rotating ball-on-three-pins configuration. A Peltier hood H-PTD 200 precisely controlled the temperature. The technical characteristics of the tribometer are presented in Table 1 and a scheme of its configuration is shown in Fig. 2. The friction tests (three replicates for each sample) were conducted at 353.15 K, being the rotational speed 213 rpm and the sliding distance 180 m. More details on the technique can be found in previous articles [26-28].

Fig. 1. Scheme of the dispersing method developed.

Table 1
Tribometer configuration, characteristics, and experimental conditions.

Ball-on-three pins configuration			
Tribology Cell T-PTD200	Tribo-pair	100Cr6 steel ball (1): 12.7 mm diameter Ra: 0.15 μm 100Cr6 pins (3): 6 mm diameter Ra: 0.3 μm	Hardness: 58–65 HRC Young's modulus: 190–210 GPa Poisson's ratio: 0.29
	Experimental conditions	0.5 mL PAO40 or dispersion (sample holder) Axial force (F) = 20 N Tribological normal force (F_N) = 9.43 N Maximum Hertzian contact pressure: 1.1 GPa Sliding distance = 180 m Rotational speed = 213 rpm	
Peltier Hood HPTD200		T = 353.15 K	

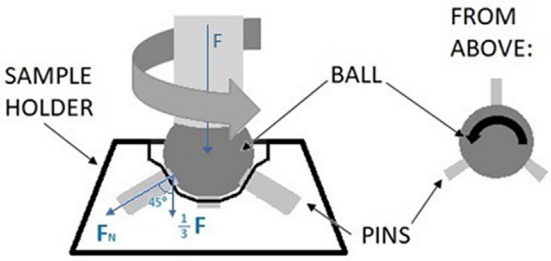

Fig. 2. Scheme of rotating ball-on-three-pins configuration.

Table 2
Profilometer measurement specifications and wear measured parameters.

Specifications	**Measured parameters**
Mode: confocal Magnification objective: 10× Software: SensoMap	Wear track width: WTW Wear track Depth: WTD Cross-sectional area: Area Surface roughness: Ra • ISO 4287 standard • Gaussian filter wavelength cut-off: 0.025 mm

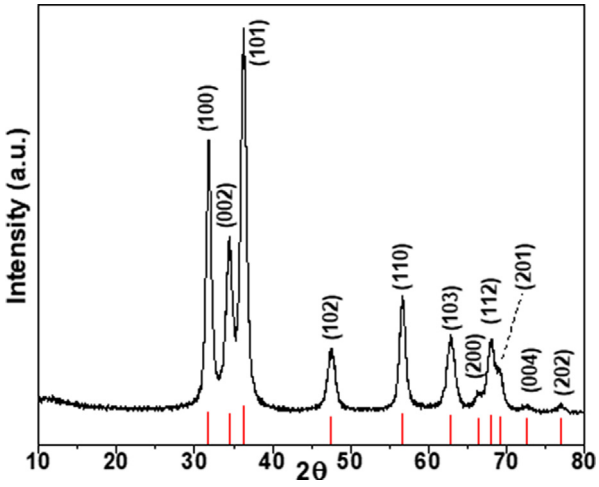

Fig. 3. Experimental XRD pattern of ZnO-OA NPs (black line) with the main peaks labelled with their corresponding Miller indices, and theoretical reflections (red bars) for zincite phase (JCPDS card No. 36–1451). (For interpretation of the references to color in this figure legend, the reader is referred to the web version of this article.)

2.3.3. Wear and roughness measurements

Once the tribological tests had been carried out, the wear produced on the pins was measured with a non-contact 3D optical profilometer (Sensofar S Neox). The specifications used in the measurements and the determined wear parameters are presented in Table 2. To understand the role of NPs in reducing wear, the wear track surface was analyzed using the confocal Raman microscope (WITec Alpha300R+). Additionally, after a tribological test with 0.25 wt% ZnO-OA + PAO40, the nanodispersion was collected to determine the final concentration of ZnO-OA NPs. For this purpose, a quantitative analysis of Zn was performed by means of an inductively coupled plasma mass spectrometer (ICP-MS), Agilent 7900x. Due to the viscous nature of the sample, an acid digestion was required. Thus, it was performed a microwave-assisted-digestion of the sample with HNO_3 at 240 °C for 30 min. Then the sample was diluted in ultrapure water. This procedure was verified with an untested 0.25 wt% ZnO-OA + PAO40 nanodispersion.

3. Results and discussion

3.1. Nanoparticle characterization

The OA content in the ZnO-OA NPs determined by TGA analysis was 65 wt%. The number of OA molecules per NP surface area unit in nm^2 was 91 ± 3. The experimental diffraction pattern of the ZnO-OA nanoparticles, obtained with XRD, together with the theoretical pattern of a hexagonal phase of zincite [29] (JCPDS card No. 36–1451) is shown in Fig. 3. The main diffraction peaks, (100), (002), (101), (102), (110), (103), (200), (112), (201), (004) and (202), perfectly matched each other.

TEM micrograph (Fig. 4a) of the oleic acid coated ZnO NPs, dispersed after synthesis in chloroform, revealed spherical NPs core with relatively inhomogeneous size distribution (medium size distribution of around 10 nm, Fig. 4b). Size distribution was performed using the ImageJ software for a sample of 200 NPs. The oleic acid coating is not observed via TEM but it adds 1.5 nm to the actual particle size.

As aforementioned, the ZnO NPs were coated with OA to facilitate their dispersibility in the base oil. The effective surface functionalization of these NPs was also analyzed by FTIR and Raman spectroscopies. The FTIR spectrum (Fig. 5) presents an absorption band at 3410 cm^{-1}, corresponding to the stretching vibrations of the O-H group attributed to the presence of hydroxyl residue, probably due to atmospheric moisture. In addition, the peaks appearing at 2923, 2853, and 722 cm^{-1} correspond to the C–H stretching vibration bands of $–CH_3$ and $–CH_2$, and the $–CH_2$ bending vibration, respectively. The peaks that appear at 1543 and 1435 cm^{-1} were assigned to the asymmetric and symmetric stretching vibrations of –COO–, respectively. The peaks at 1543

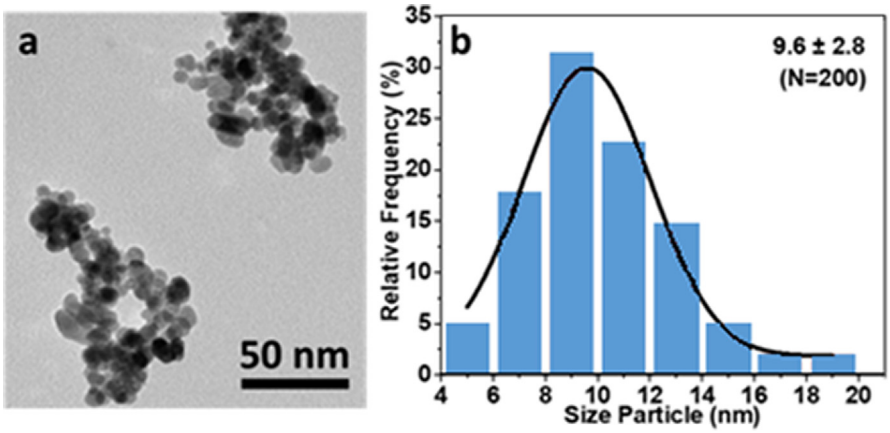

Fig. 4. TEM micrograph (a) and the size distribution (b) of the core of the ZnO-OA NPs.

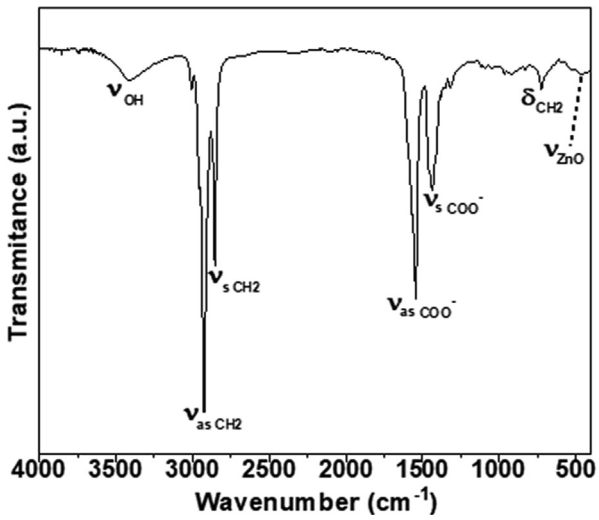

Fig. 5. FTIR spectrum of ZnO-OA with the characteristic bands as evidence.

and 1435 cm^{-1} were assigned to the asymmetric and symmetric stretch vibrations of –COO–, respectively. Finally, the vibration band observed at 468 cm^{-1} corresponds to the stretching vibration of the zincite structure (Zn-O) [30]. These findings confirmed that ZnO NPs were successfully coated with oleic acid. It is worth mentioning that the FTIR spectrum of Fig. 5 is very similar to that reported by Wu et al. [12] for other ZnO-OA NPs.

The ZnO-OA NPs Raman spectrum is shown in Fig. S1 of the Supplementary Information. As expected, the signals corresponding to oleic acid were identified: a Raman band around 2800–3000 cm^{-1} corresponding to symmetric and asymmetric stretching of CH_2, other CH_2 peaks at 1447 and 1306 cm^{-1} corresponding to scissoring and twisting, respectively, a CH_3 rocking peak at 879 cm^{-1}, several peaks at 1068, 1090 and 1117 cm^{-1}corresponding to C-C vibration, as well as peaks related with the C = C double bond, at 3008 cm^{-1} from = C-H vibration peak, 1663 cm^{-1} corresponding to C = C vibration, and 1268 and 971 cm^{-1} assignable to C = C-H bending peaks. Nevertheless, the peaks corresponding to ZnO were not clearly detected, likely due to the high oleic acid content [31,32].

3.2. Nanolubricants stability

The PAO40 + 0.25 wt% ZnO-OA dispersion had good stability features (Fig. 6). The appearance of the dispersion was monitored by recording photographs since immediately after the dispersion sonication (time 0 h). The dispersion started to be less transparent 29 days after sonication. Refractive index of PAO40 and the nanolubricant are shown in Fig. 7 at 298.15 K. The evolution of the refractive index followed a near-to-zero slope close to that of the neat PAO40. After 45 h, the relative increase of the refractive index was 0.013%, which was 10 times lower to that of the PAO40 + 0.0 5 wt% h-BN dispersion reported in a previous work [21]. From all the above results it can be concluded that the ZnO-OA NPs have around one-month stability in PAO40 at 0.25 wt% concentration. To analyze the effect of the OA coating on the stability results a 0.25 wt% ZnO dispersion in PAO40 was prepared. Although the preparation method explained in Fig. 1 was attempted, it did not work because of the poor dispersibility of the uncoated ZnO NPs in $CHCl_3$, forming a bulky agglomerate that did not disappear even after bath or tip ultrasonication, as shown in Fig. 6b. To solve this problem, it was necessary to dry the NPs and to prepare the dispersion using a two-step method [6], consisting of adding the dried ZnO nanopowder to the PAO40 followed by a homogenization step in an ultrasonic bath for 4 h. The attempt to prepare a homogeneous dispersion of PAO40 + 0.25 wt% ZnO was also unsuccessful as the uncoated ZnO NPs did not disperse in the base oil. After 4 h in the ultrasonic bath, these NPs were still aggregated at the bottom of the glass flask, due to their strong oleophobicity, as shown in Fig. 6c. Thus, when the container was turned over, it was seen how aggregates fall.

3.3. Thermophysical characterization

Nanodispersions density, ρ, measured with SVM 3000 Stabinger equipment, showed a slight increment with the mass concentration of NPs, as summarized in Fig. 8 and Table S1. Thus, the ZnO-OA nanodispersions at 0.10, 0.25, 0.50, 0.75 and 1.00 wt% caused a relative increase respect to the PAO40 density of approx. 0.1%, 0.2%, 0.3%, 0.4% and 0.5%, respectively. Some authors [16] attributed the increase in the nanofluid density with the concentration of NPs to their agglomeration, however the density increase may be simply because the density of the ZnO-OA NPs is greater than that of PAO40.

The densities of the nanodispersions have been estimated with the Pak and Cho [34] and Wasp et al. [35] empirical equations (equations S2 and S3, respectively, of the supplementary material). For each composition, the absolute average deviations (AAD%) obtained with the Pak and Cho model between experimental and predicted densities in the whole temperature range is lower than 0.25% being the maximum deviation 0.28%. Worse results have been obtained with the equation due to Wasp et al. [35] (equation

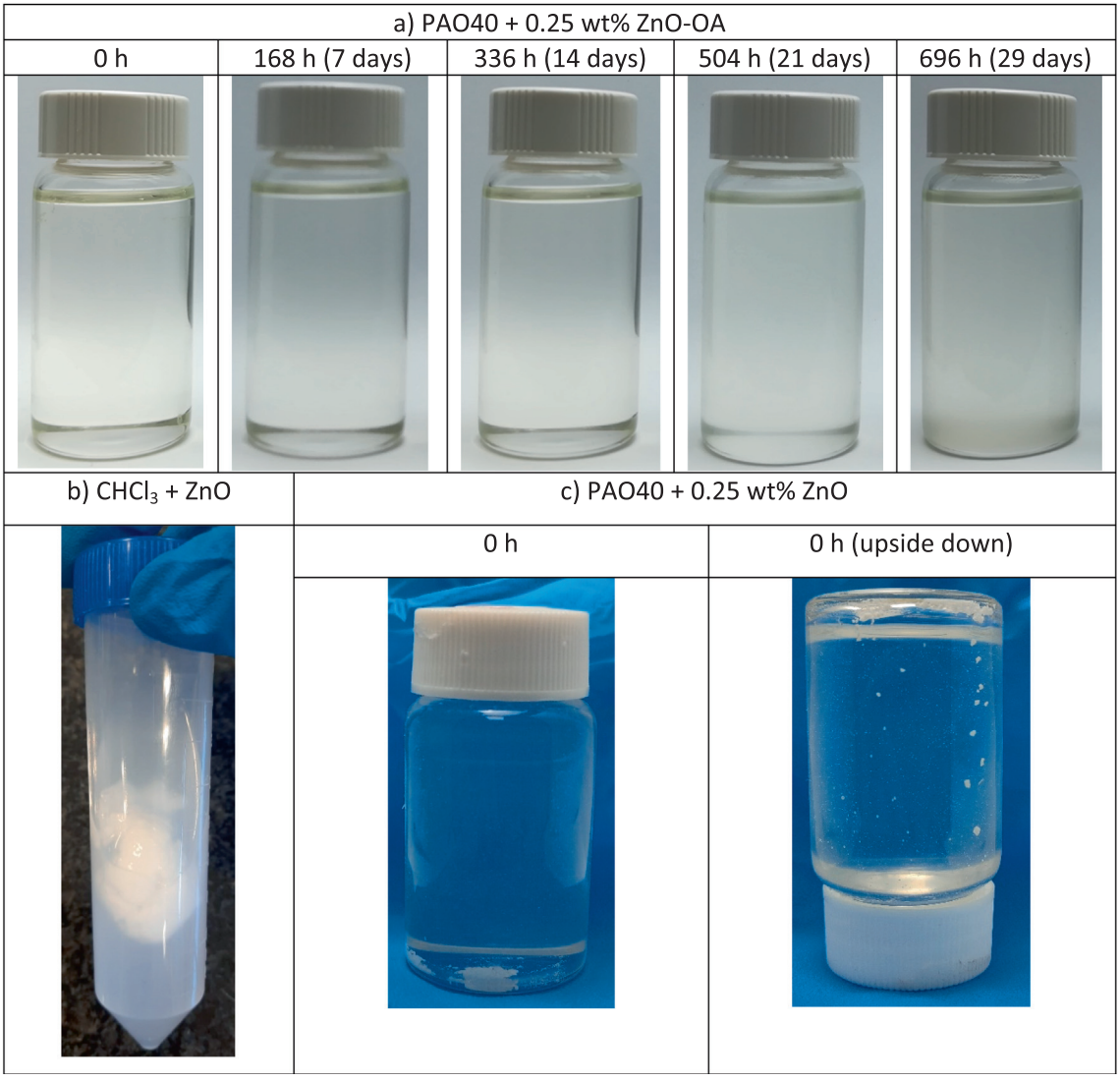

Fig. 6. Photographs of PAO40 + 0.25 wt% ZnO-OA (a), $CHCl_3$ + ZnO (b) and PAO40 + 0.25 wt% ZnO (c) showing visual stability up to 696 h.

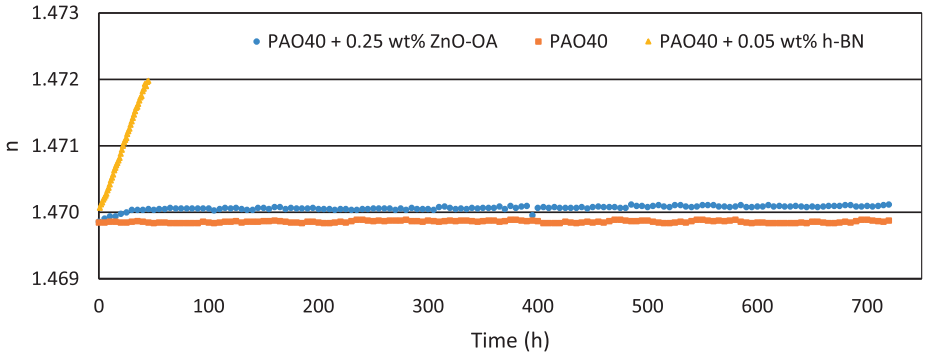

Fig. 7. Evolution of refractive index, n, with time of PAO40 (orange), PAO40 + 0.25 wt% ZnO-OA (blue) and PAO40 + 0.05 wt% h-BN (yellow, [21]) at 298.15 K. Error bars are smaller than the size of the symbols. (For interpretation of the references to color in this figure legend, the reader is referred to the web version of this article.)

S3), being 0.42% the maximum AAD%, corresponding to the nanodispersion with 1.00 wt% ZnO-OA mass fraction. In Fig. S3, the predicted densities have been plotted together with the experimental ones.

Regarding dynamic viscosity, its relative changes caused by the addition of the ZnO-OA NPs to the PAO40 are shown in Fig. 9. Table S2 gathers the experimental dynamic viscosity values of PAO40 and the nanolubricants. Viscosities increased up to 4% with the concentration of ZnO-OA NPs due to the enhancement of the internal shear stress of the nanolubricants, i.e., the increase of internal friction [36]. As in the case of densities, the nanodispersion viscosities have been predicted by three empirical models: the Einstein equation [37] (eq. S4), that due to Pak and Cho [34] (eq. S5) and the one proposed by Chen et al. [38] (eq. S6). Despite its sim-

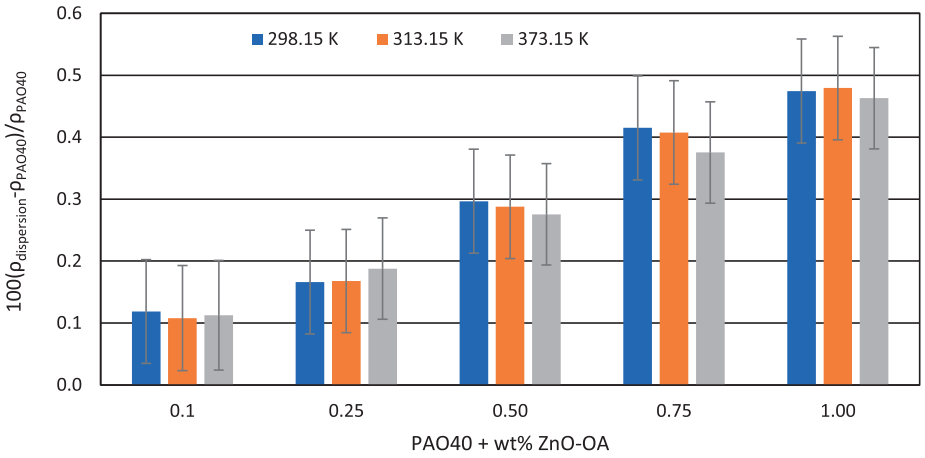

Fig. 8. Percentage variation of density between ρ values of the dispersions at different concentrations of ZnO-OA ($\rho_{dispersion}$) with respect to neat PAO40 (ρ_{PAO40}) at 298.15, 313.15 and 373.15 K.

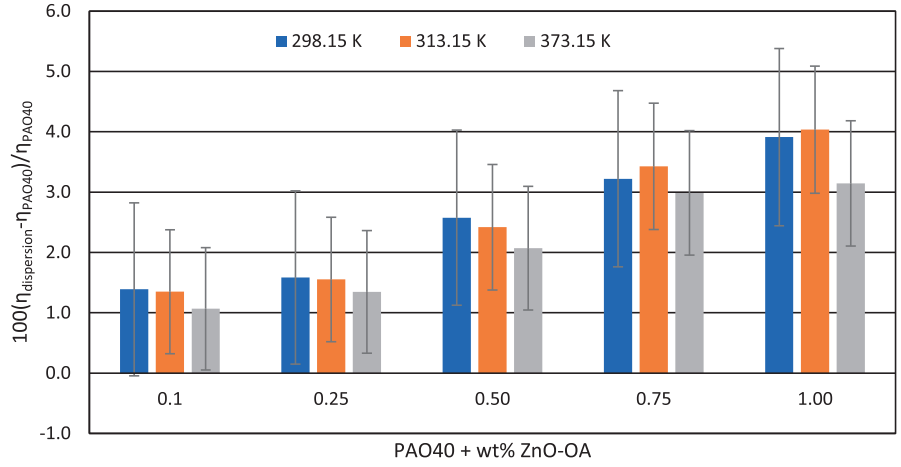

Fig. 9. Percentage variation of the dynamic viscosity (η) corresponding to the different PAO40 + ZnO-OA dispersions ($\eta_{dispersion}$) with respect to that of neat PAO40 (η_{PAO40}), at 298.15, 313.15 and 373.15 K.

plicity, the equation due to Einstein predicts experimental viscosities with AAD% lower than 2.9%. The worse results are those provided by Pak and Cho model [34] (AAD% lower than 7.3%). The best results are those provided by Chen et al. equation [38], with AADs lower than 0.87%. In Fig. S4 the predicted viscosities are plotted together with the experimental ones.

According with the Carreau parameters reported for PAO40 [39], up to very high shear rates at 0.1 MPa (from $2{\cdot}10^6$ s^{-1} at 298.15 K to $3{\cdot}10^7$ s^{-1} at 373.15 K), its behavior is Newtonian. These shear rates are much higher than those applied when using SVM3000 apparatus, which remain between 10 and 10^3 s^{-1}, being dependent on the fluid viscosity [40]. So, taking these facts into account and the small influence of the addition of nanoparticles on the viscosity (lower than 4%) in the range of concentrations analyzed, it is expected that the nanodispersions do not display any shear thinning in the shear conditions of the viscosity measurements.

Finally, the measured viscosity indices (VI) of the nanodispersions were slightly lower than that of PAO40 and remained approximately constant regardless of the composition as shown in Fig. 10.

3.4. Tribological characterization

The friction results of the ball-on-three pins tests for PAO40 and all the ZnO-OA nanodispersions are summarized in Table 3 and presented in Fig. 11. The five studied dispersions decreased the coefficient of friction compared to the neat PAO40, ranging from 14% to 25%. The lowest friction value was achieved when 0.25 wt % ZnO-OA was added to PAO40; a further increase on nanoparticle concentration resulted in worse friction reduction. Therefore, based on these results, the optimal ZnO-OA concentration for friction coefficient reduction was 0.25 wt%. Minima in the friction-concentration curves for several nanolubricants were previously reported by different authors [41–45,52].

3.5. Wear surface characterization

Regarding the wear track depth (WTD) at the surface of the pins (Fig. 11), the best antiwear performance was also obtained for the nanolubricant prepared with 0.25 wt% ZnO-OA NPs. Dispersions with lower concentrations did not have enough NPs to minimize friction and wear. On the other hand, for higher NP concentrations, ZnO-OA nanoparticles or aggregates could act as debris particles, increasing friction and wear [46]. Mean values of various wear parameters and their respective standard deviations, such as wear track width (WTW), depth (WTD), and cross-sectional area of the worn pins are summarized in Table 4. The greatest reductions for these wear parameters were also found with the PAO40 + 0.25 wt % ZnO-OA nanodispersion, being 38%, 68% and 82%, in WTW, WTD and cross-sectional area, respectively.

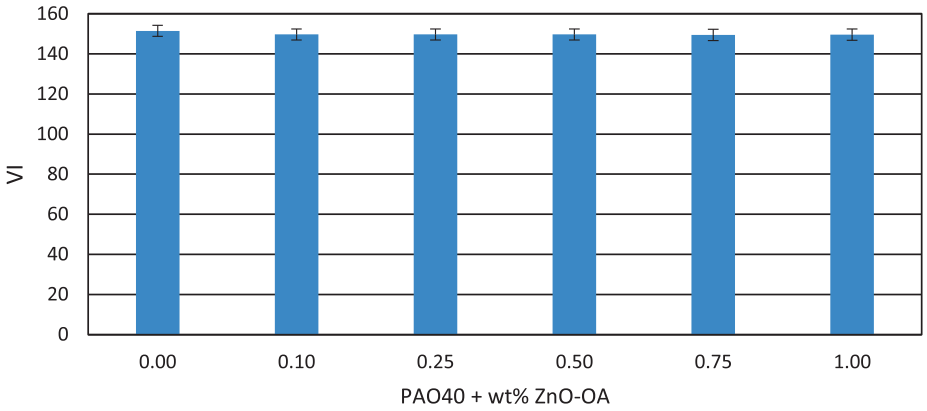

Fig. 10. Comparison of viscosity indices (VI) for neat PAO40 and PAO40 + ZnO-OA dispersions with different weight percentages (wt%) of ZnO-OA.

Table 3
Average friction coefficient values, μ, at 353.15 K and their standard deviations, σ, for PAO40 base oil and PAO40 + wt% ZnO-OA lubricants at different NP weight percentages, wt%.

wt%	μ	σ	Reduction%
0	0.0938	0.0027	–
0.10	0.0721	0.0028	23
0.25	0.0701	0.0022	25
0.50	0.0757	0.0032	19
0.75	0.0765	0.0012	18
1.00	0.0802	0.0023	14

2D images and 3D profiles of the worn pins are shown in Fig. 12. Wear was strongly reduced as evidenced when comparing a pin tested with PAO40 (Fig. 12a and 12b) with a pin tested with PAO40 + 0.25 wt% ZnO-OA (Fig. 12c and 12d). Furthermore, the wear reductions were also evident in the cross-sectional profiles of those same worn pins in Fig. 13.

The roughness (Ra) of wear tracks was another parameter measured by 3D profilometry to analyze the anti-wear capability of the nanolubricants. The surface roughness of the unused pins was also characterized. The mean values of the roughness are shown in Fig. 14 for worn and unused pins. All nanodispersions, except for 1.00 wt% ZnO-OA in PAO40, provided worn surfaces with lower Ra values than those of the unused pins, however, only the dispersions with the two lowest NP concentrations (0.1 and 0.25 wt%) had better polishing performances than that of neat PAO40, obtaining the optimal Ra value for 0.25 wt% ZnO-OA dispersion, which reduced the Ra value by 67% compared to that of the unused pin surface and 43% compared to that lubricated with PAO40.

Raman spectra of ZnO-OA (Fig. S1) and of PAO40 (Fig. S2) are very similar due to the structural similarity of both compounds containing C-C bonds and $-CH_2$ groups. Nevertheless, there were two clear differences in the case of oleic acid (Fig. S1): there was a C = C signal at 1663 cm^{-1} due to the vibration of the double bond and another signal at 3008 cm^{-1} corresponding to vibration = C-H, which did not appear in the PAO40 spectrum. Raman maps of the worn pin surfaces were also recorded. To distinguish between PAO40 and ZnO-OA in the Raman maps of these surfaces, the dissimilar peak at 1663 cm^{-1} of the ZnO-OA spectrum was used to identify the presence of these NPs. Similar procedure has been used previously by Nasser at al. [26,47,48] to discriminate between the PAO32 Raman spectrum and those of three ionic liquids.

From the Raman map corresponding to the worn pin surface lubricated with neat PAO40 (Fig. 15), the presence of PAO40 (red area), iron oxides (blue area) as well as small and scarce carbon areas (yellow) were evidenced. These results agree with those found by Ratoi et al. [49] from XPS measurements on a disk wear track obtained with PAO6 from ball-on-disk tribological tests at 393.15 K, using a similar tribo-pair. These authors concluded that the tribofilm built up on the wear track was mainly formed by carbon, iron, and oxygen, and thus the smooth wear could be due to oxide formation and lubricant degradation on the wear track among other effects. In addition, recently, from confocal Raman microscopy, Nasser et al. [26] also found for a similar pin worn surface tested with PAO32 at 353.15 K; namely, the boundary

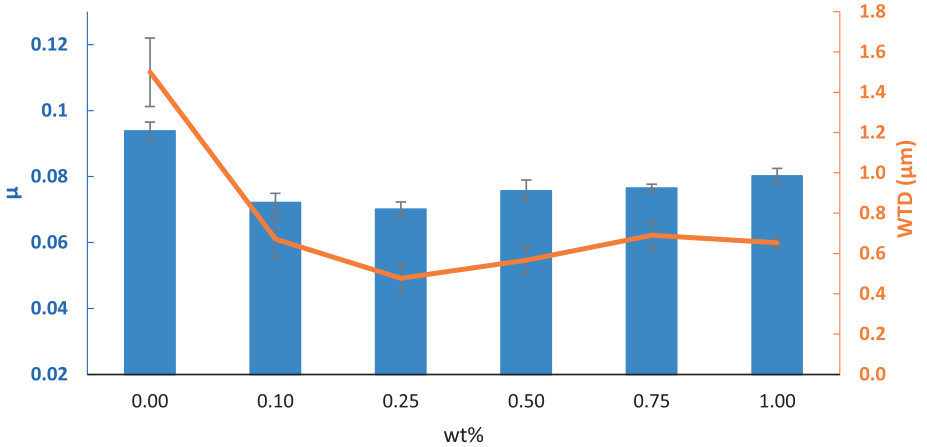

Fig. 11. Average friction coefficient, μ, (blue) and wear track depth, WTD, (orange) for PAO40 and PAO40 + wt% ZnO-OA nanodispersions for different NP weight percentages, wt%. (For interpretation of the references to color in this figure legend, the reader is referred to the web version of this article.)

Table 4
Average values of the width, WTW, depth, WTD, and cross-sectional area of the wear track and their standard deviations for PAO40 + wt% ZnO-OA lubricants for different NP weight percentages, wt%.

wt%	WTW/μm	σ/μm	WTD/μm	σ/μm	Area/μm^2	σ/μm^2
0	370	7	1.50	0.17	411	54
0.10	269	15	0.67	0.10	119	36
0.25	230	14	0.48	0.07	75	18
0.50	241	15	0.57	0.07	78	14
0.75	289	29	0.69	0.07	96	22
1.00	259	25	0.65	0.03	119	31

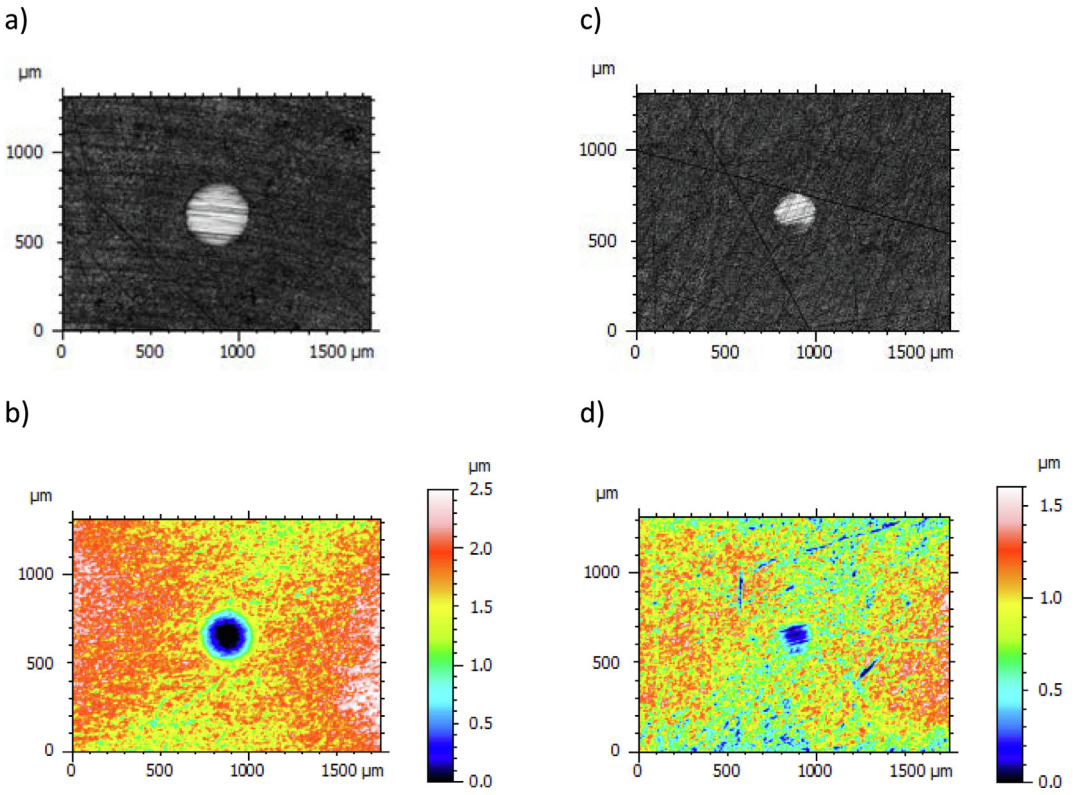

Fig. 12. 2D Images and 3D profiles of the wear tracks in the pins tested with neat PAO40 (a, b) and with its nanolubricant containing 0.25 wt% ZnO-OA (c, d).

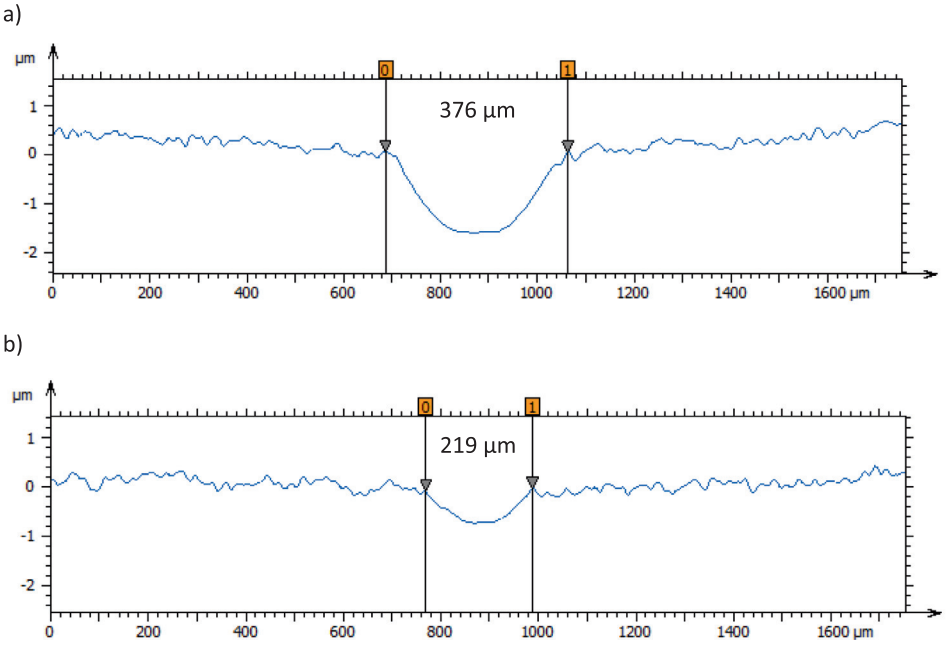

Fig. 13. Cross-sectional profiles of the wear tracks on the pins lubricated with neat PAO40 (a) PAO40 + 0.25 wt% ZnO-OA (b).

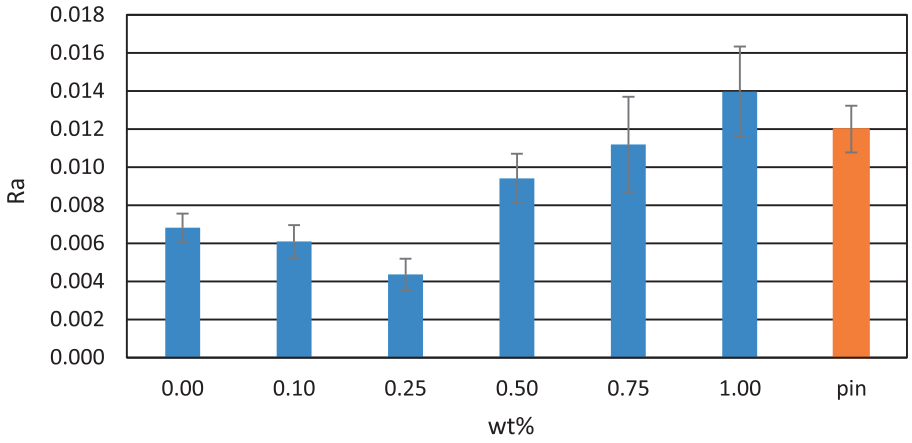

Fig. 14. Roughness (Ra) of the unused pin surface (orange) and of the worn pin surfaces (blue) tested with PAO40 and PAO40 + wt% ZnO-OA nanodispersions with different NP weight percentages, wt%. (For interpretation of the references to color in this figure legend, the reader is referred to the web version of this article.)

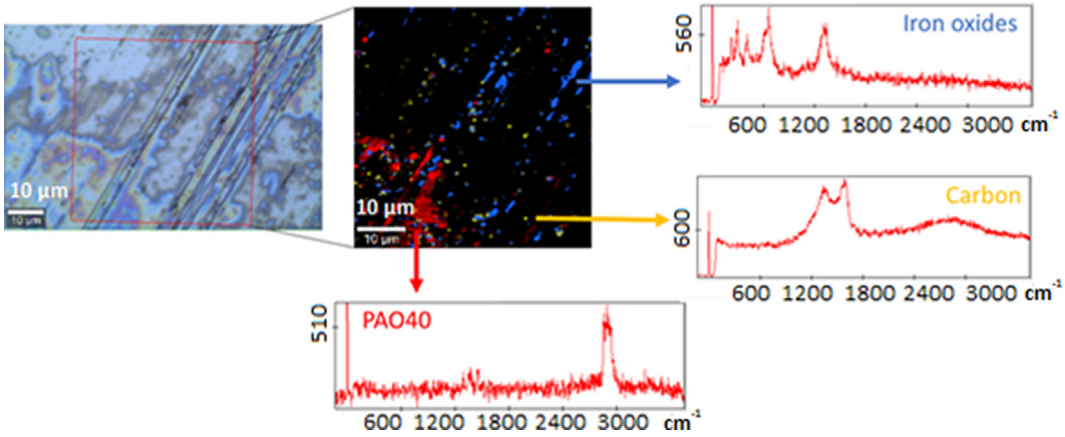

Fig. 15. Raman map of the worn pin surface tested with PAO40 and spectra of the components present on this surface: PAO40 (red), carbon (yellow) and iron oxides (blue). (For interpretation of the references to color in this figure legend, the reader is referred to the web version of this article.)

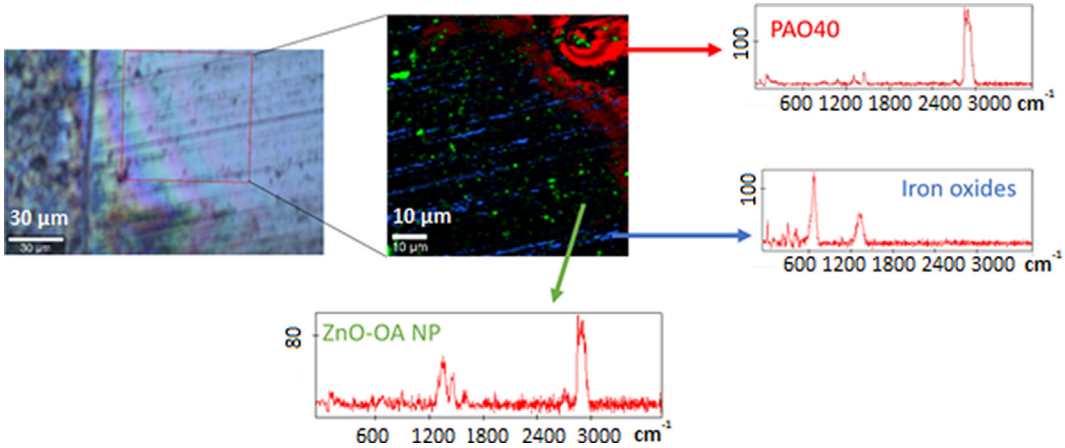

Fig. 16. Raman map of the worn pin surface tested with PAO40 + 0.25 wt% ZnO-OA and spectra of the components present on that surface: PAO40 (red), carbon (yellow) and iron oxides (blue). (For interpretation of the references to color in this figure legend, the reader is referred to the web version of this article.)

tribofilms were composed of iron oxides, carbon, and the oil itself.

Raman map on the worn surface tested with PAO40 + 0.25 wt% ZnO-OA (Fig. 16) shows the presence of PAO40 (red color), oleic acid, i.e., ZnO-OA nanoparticles, (green color) and iron oxides (blue color). The obtained signals of the ZnO-OA nanoparticles in the worn scar overlapped with those of another component, probably carbon, which appeared also in the worn surfaces of neat PAO40

(Fig. 15, yellow color). The presence of the ZnO-OA nanoparticles in the worn scar tribofilm was also shown in the ICP-MS analysis of the nanolubricant collected after the tribotest. This nanolubricant contains 0.21 wt% of ZnO-OA NPs, i.e., a 16% reduction.

Regarding the tribological mechanisms, both rolling and mending effects could be behind the better tribological performance of nanolubricants with respect to that of neat PAO40. Rolling may transform sliding friction into rolling friction as a result of the spherical shape of ZnO-OA NPs (Fig. 4, [50,51]). The mending effect was evidenced by the presence of small areas of ZnO-OA NPs in the Raman maps of the contact surfaces and by the decrease of their roughness, as well as by the slight loss of ZnO-OA NPs in the nanolubricant after the tribotest. Raman mapping also evidenced the presence of big PAO40 tribofilms.

4. Conclusions

The features achieved in this work can be summarized as:

The synthesis and coating with oleic acid of ZnO NPs were carried out successfully. The oleic acid coated ZnO (ZnO-OA) NPs, with a mean diameter around 10 nm, were characterized by XRD (the nanoparticle core) and FTIR (the coating).

Using as neat base oil PAO40, five nanolubricants with ZnO-OA concentrations ranging from 0.10 to 1.00 wt% were designed as well as thermophysically and tribologically characterized.

Density increases roughly linearly with the mass concentration of NPs, reaching 0.5% for nanodispersion with 1.00 wt% ZnO-OA. Dynamic viscosities also increase with the concentration of NPs, with relative increases of up to 4.0% for the base oil additivated with 1 wt% of ZnO-OA. On the contrary, viscosity indices barely vary with the nanoparticle concentration, being slightly lower than that of PAO40.

At 353.15 K, all the nanolubricants improve the tribological behavior of PAO40, being the optimal concentration 0.25 wt% of ZnO-OA (25% of reduction in the friction coefficient and wear reductions up to 82% in the case of cross sectional area, respect to those obtained with the neat base oil).

The better tribological performance of the nanolubricants respect to that of neat PAO40 could be due to the occurrence of rolling and mending mechanisms owing to the spherical shape and the adsorption of the additives on the rubbed steel surfaces.

From confocal Raman microscopy on the worn surfaces obtained from tribological test as well as from the ICP-MS results with PAO40 + 0.25 wt% ZnO-OA dispersion, it is illustrated the built up of tribofilm composed by PAO40, oleic acid i.e., ZnO-OA NPs, and iron oxides.

CRediT authorship contribution statement

Fátima Mariño: Investigation, Formal analysis, Writing – original draft. **Enriqueta R. López:** Methodology, Conceptualization, Writing – review & editing, Validation, Supervision. **Ángela Arnosa:** Investigation, Validation. **Manuel A. González Gómez:** Methodology, Validation. **Yolanda Piñeiro:** Conceptualization, Writing – review & editing, Supervision. **José Rivas:** Resources, Supervision. **Carmen Alvarez-Lorenzo:** Resources, Supervision, Writing – review & editing. **Josefa Fernández:** Project administration, Funding acquisition, Conceptualization, Writing – review & editing.

Declaration of Competing Interest

The authors declare that they have no known competing financial interests or personal relationships that could have appeared to influence the work reported in this paper.

Acknowledgments

The authors thank Repsol for providing the PAO40 sample. The authors are grateful for the use of the RIAIDT-USC analytical facilities, especially Mr. Ezequiel Vázquez for his valuable help with Raman analyzes. Funding for this work has been provided by the Ministry of Science, Innovation and Universities of Spain and the European Regional Development Fund (ERDF, FEDER in Spanish) through the ENE2017-86425-C2-2-R project, and by the Xunta de Galicia through ED431C 2020/10.

Appendix A. Supplementary data

Supplementary data to this article can be found online at https://doi.org/10.1016/j.molliq.2021.118401.

References

[1] M. Kandeva, V. Majstorović, E. Assenova, Tribology enhancement of lubricant quality and safety, Int. J. Total Quality Manage. Excellence 42 (2014).
[2] K. Holmberg, A. Erdemir, The impact of tribology on energy use and CO_2 emission globally and in combustion engine and electric cars, Tribol. Int. 135 (2019) 389–396, https://doi.org/10.1016/j.triboint.2019.03.024.
[3] K. Holmberg, A. Erdemir, Influence of tribology on global energy consumption, costs and emissions, Friction 5 (3) (2017) 263–284, https://doi.org/10.1007/s40544-017-0183-5.
[4] L.I. Farfan-Cabrera, Tribology of electric vehicles: a review of critical components, current state and future improvement trends, Tribol. Int. 138 (2019) 473–486, https://doi.org/10.1016/j.triboint.2019.06.029.
[5] W.R. Murphy, D.A. Blain, A.S. Galiano-Roth, P.A. Galvin, Benefits of synthetic lubricants in industrial applications, J. Synth. Lubr. 18 (4) (2002) 301–325, https://doi.org/10.1002/jsl.3000180406.
[6] N.F. Azman, S. Samion, Dispersion stability and lubrication mechanism of nanolubricants: a review, Int. J. Precis. Eng. Manuf. 6 (2) (2019) 393–414, https://doi.org/10.1007/s40684-019-00080-x.
[7] J. Patel, A. Kiani, Effects of reduced graphene oxide (rGO) at different concentrations on tribological properties of liquid base lubricants, Lubricants 7 (2019) 11.
[8] B. Li, X. Wang, W. Liu, Q. Xue, Tribochemistry and antiwear mechanism of organic–inorganic nanoparticles as lubricant additives, Tribol. Lett. 22 (1) (2006) 79–84, https://doi.org/10.1007/s11249-005-9002-7.
[9] D.-X. Peng, C.-H. Chen, Y. Kang, Y.-P. Chang, S.-Y. Chang, Size effects of SiO_2 nanoparticles as oil additives on tribology of lubricant, Ind. Lubrication Tribology 62 (2) (2010) 111–120, https://doi.org/10.1108/00368791011025656.
[10] J. Zhao, Y. Huang, Y. He, Y. Shi, Nanolubricant additives: A review, Friction 9 (5) (2021) 891–917, https://doi.org/10.1007/s40544-020-0450-8.
[11] S.B. Mousavi, S. Zeinali Heris, P. Estellé, Viscosity, tribological and physicochemical features of ZnO and MoS_2 diesel oil-based nanofluids: An experimental study, Fuel 293 (2021) 120481, https://doi.org/10.1016/j.fuel.2021.120481.
[12] L. Wu, Y. Zhang, G. Yang, S. Zhang, L. Yu, P. Zhang, Tribological properties of oleic acid-modified zinc oxide nanoparticles as the lubricant additive in poly-alpha olefin and diisooctyl sebacate base oils, Royal Soc. Chem. Adv. 6 (2016) 69836–69844, https://doi.org/10.1039/C6RA10042BB.
[13] Y. Chen, P. Renner, H. Liang, Dispersion of nanoparticles in lubricating oil: A critical review, Lubricants 7 (2019) 7, https://doi.org/10.3390/lubricants7010007.
[14] A. Hernandez Battez, J.E. Fernandez Rico, A. Navas Arias, J.L. Viesca Rodriguez, R. Chou Rodriguez, J.M. Diaz Fernandez, The tribological behaviour of ZnO nanoparticles as an additive to PAO6, Wear 261 (3-4) (2006) 256–263.
[15] L. Gara, Q. Zou, Friction and wear characteristics of oil-based ZnO nanofluids, Tribol. Trans. 56 (2) (2013) 236–244.
[16] S. Kannaiyan, C. Boobalan, A. Umasankaran, A. Ravirajan, S. Sathyan, T. Thomas, Comparison of experimental and calculated thermophysical properties of alumina/cupric oxide hybrid nanofluids, J. Mol. Liq. 244 (2017) 469–477, https://doi.org/10.1016/j.molliq.2017.09.035.
[17] J.M. Liñeira del Río, E.R. López, M. González Gómez, S. Yañez Vilar, Y. Piñeiro, J. Rivas, D.E. Gonçalves, J.H. Seabra, J. Fernández, Tribological behavior of nanolubricants based on coated magnetic nanoparticles and trimethylolpropane trioleate base oil, J. Nanomater. 10 (2020) 683, https://doi.org/10.3390/nano10040683.
[18] D. Coronado, J. Wenske, Monitoring the oil of wind-turbine gearboxes: main degradation indicators and detection methods, Machines 6 (2018) 25, https://doi.org/10.3390/machines6020025.
[19] R.J. Andrade Vieira, M.Á. Sanz Bobi, Evaluación de Indicadores de la Condición de Aerogeneradores, Anales de Mecánica y Electricidad 90 (2013) 17-26 www.iit.comillas.edu/docs/IIT-13-030A.pdf.
[20] M.A. Coelho de Sousa Marques, M.J.G. Guimarey, V. Domínguez-Arca, A. Amigo, J. Fernández, Heat capacity, density, surface tension, and contact angle for

polyalphaolefins and ester lubricants, Thermochim. Acta 703 (2021) 178994, https://doi.org/10.1016/j.tca.2021.178994.
[21] J.M. Liñeira del Río, E.R. López, J. Fernández, Tribological properties of graphene nanoplatelets or boron nitride nanoparticles as additives of a polyalphaolefin base oil, J. Mol. Liq. 333 (2021) 115911, https://doi.org/10.1016/j.molliq.2021.115911.
[22] N.M. Shamhari, B.S. Wee, S.F. Chin, K.Y. Kok, Synthesis and characterization of zinc oxide nanoparticles with small particle size distribution, Acta Chim. Slov. 65 (2018) 578–585. https://doi.org/10.17344/acsi.2018.4213.
[23] K. Granados, J. Gracia-Fadrique, A. Amigo, R. Bravo, Refractive index, surface tension, and density of aqueous mixtures of carboxylic acids at 298.15 K, J. Chem. Eng. Data 51 (4) (2006) 1356–1360, https://doi.org/10.1021/je060084c.
[24] F.M. Gaciño, T. Regueira, L. Lugo, M.J.P. Comuñas, J. Fernández, Influence of Molecular Structure on Densities and Viscosities of Several Ionic Liquids, J. Chem. Eng. Data 56 (12) (2011) 4984–4999, https://doi.org/10.1021/je200883w.
[25] ASTM D2270 2016 Standard practice for calculating viscosity index from kinematic viscosity at 40 and 100 °C.
[26] K.I. Nasser, J.M. Liñeira del Río, E.R. López, J. Fernández, Synergistic effects of hexagonal boron nitride nanoparticles and phosphonium ionic liquids as hybrid lubricant additives, J. Mol. Liq. 311 (2020) 113343, https://doi.org/10.1016/j.molliq.2020.113343.
[27] M.J.G. Guimarey, A.M. Abdelkader, M.J.P. Comuñas, C. Alvarez-Lorenzo, B. Thomas, J. Fernández, M. Hadfield, Comparison between thermophysical and tribological properties of two engine lubricant additives: electrochemically exfoliated graphene and molybdenum disulfide nanoplatelets, J. Nanotechnol. 32 (2) (2021) 025701, https://doi.org/10.1088/1361-6528/abb7b1.
[28] J.P. Vallejo, J.M. Liñeira del Río, J. Fernández, L. Lugo, Tribological performance of silicon nitride and carbon black Ionanofluids based on 1-ethyl-3-methylimidazolium methanesulfonate, J. Mol. Liq. 319 (2020) 114335, https://doi.org/10.1016/j.molliq.2020.114335.
[29] Y.T. Prabhu, K.V. Rao, V.S.S. Kumar, B.S. Kumari, Synthesis of ZnO nanoparticles by a novel surfactant assisted amine combustion method, Adv. Nanoparticles 02 (01) (2013) 45–50, https://doi.org/10.4236/anp.2013.21009.
[30] R. Hong, T. Pan, J. Qian, H. Li, Synthesis and surface modification of ZnO nanoparticles, Chem. Eng. J. 119 (2-3) (2006) 71–81, https://doi.org/10.1016/j.cej.2006.03.003.
[31] M. Yoshikawa, K. Inoue, T. Nakagawa, H. Ishida, N. Hasuike, H. Harima, Characterization of ZnO nanoparticles by resonant Raman scattering and cathodoluminescence spectroscopies, Appl. Phys. Lett. 92 (11) (2008) 113115, https://doi.org/10.1063/1.2901159.
[32] M. Šćepanović, M. Grujić-Brojčin, K. Vojisavljević, S. Bernik, T. Srećković, Raman study of structural disorder in ZnO nanopowders, Raman Spectroscopy 41 (9) (2010) 914–921, https://doi.org/10.1002/jrs.2546.
[34] B.C. Pak, Y.I. Cho, Hydrodynamic and heat transfer study of dispersed fluids with submicron metallic oxide particles, Exp. Heat Transfer 11 (2) (1998) 151–170, https://doi.org/10.1080/08916159808946559.
[35] E.J. Wasp, J.P. Kenny, R.L. Gandhi, Solid-liquid flow slurry pipeline transportation, 1979.
[36] A. Ahmadi Nadooshan, M. Hemmat Esfe, M. Afrand, Evaluation of rheological behavior of 10W40 lubricant containing hybrid nano-material by measuring dynamic viscosity, Physica E 92 (2017) 47–54, https://doi.org/10.1016/j.physe.2017.05.011.
[37] A. Einstein, Eine neue bestimmung der molekuldimensionen, Ann. Phys. 34 (1911) 591–592, https://doi.org/10.1002/andp.19063240204.
[38] H. Chen, Y. Ding, C. Tan, Rheological behaviour of nanofluids, New J. Phys. 9 (2007) 367 https://doi.org/10.1088/1367-2630/9/10/367.
[39] S. Bair, High pressure rheology for quantitative elastohydrodynamics, second ed., Elsevier, 2019.
[40] N. Marx, L. Fernández, F. Barceló, H. Spikes, Shear thinning and hydrodynamic friction of viscosity modifier-containing oils. Part I: shear thinning behaviour, Tribol. Lett. 66 (2018) 1-14 https://doi.org/10.1007/s11249-018-1039-5.
[41] L. Wu, Y. Zhang, G. Yang, S. Zhang, L. Yu, P. Zhang, Tribological properties of oleic acid-modified zinc oxide nanoparticles as the lubricant additive in poly-alpha olefin and diisooctyl sebacate base oils, RSC Adv. 6 (74) (2016) 69836–69844, https://doi.org/10.1039/C6RA10042B.
[42] V. Zin, S. Barison, F. Agresti, L. Colla, C. Pagura, M. Fabrizio, Improved tribological and thermal properties of lubricants by graphene based nano-additives, Royal Soc. Chem. Adv. 6 (64) (2016) 59477–59486, https://doi.org/10.1039/C6RA12029F.
[43] L. Liu, Z. Fang, A. Gu, Z. Guo, Lubrication effect of the paraffin oil filled with functionalized multiwalled carbon nanotubes for bismaleimide resin, Tribol. Lett. 42 (1) (2011) 59–65, https://doi.org/10.1007/s11249-011-9749-y.
[44] J.M. Liñeira del Río, M.J.G. Guimarey, M.J.P. Comuñas, E.R. López, A. Amigo, J. Fernández, Thermophysical and tribological properties of dispersions based on graphene and a trimethylolpropane trioleate oil, J. Mol. Liq. 268 (2018) 854–866, https://doi.org/10.1016/j.molliq.2018.07.107.
[45] B. Gupta, N. Kumar, K. Panda, S. Dash, A. Tyagi, Energy efficient reduced graphene oxide additives: Mechanism of effective lubrication and antiwear properties, Sci. Rep. 6 (2016) 1–10, https://doi.org/10.1038/srep18372.
[46] N.A. Ismail, S. Bagheri, Highly oil-dispersed functionalized reduced graphene oxide nanosheets as lube oil friction modifier, Mater. Sci. Eng., B 222 (2017) 34–42, https://doi.org/10.1016/j.mseb.2017.04.010.
[47] K.I. Nasser, J.M. Liñeira del Río, E.R. López, J. Fernández, Hybrid combinations of graphene nanoplatelets and phosphonium ionic liquids as lubricant additives for a polyalphaolefin, J. Mol. Liq. 336 (2021) 116266, https://doi.org/10.1016/j.molliq.2021.116266.
[48] K.I. Nasser, J.M. Liñeira del Río, F. Mariño, E.R. López, J. Fernández, Double hybrid lubricant additives consisting of a phosphonium ionic liquid and graphene nanoplatelets/hexagonal boron nitride nanoparticles, Tribol. Int. 163 (2021) 107189, https://doi.org/10.1016/j.triboint.2021.107189.
[49] M. Ratoi, H. Tanaka, B.G. Mellor, J. Sugimura, Hydrocarbon lubricants can control hydrogen embrittlement, Sci. Rep. 10 (2020) 1361, https://doi.org/10.1038/s41598-020-58294-y.
[50] D. Singh, U. Bhan, P.K. Painuly, Effect of ZnO nanoparticles concentration on the friction and wear behaviour of Mahua oil, Mater. Today:. Proc. 46 (2020) 10117–10120, https://doi.org/10.1016/j.matpr.2020.09.379.
[51] M.K.A. Ali, X. Hou, M.A.A. Abdelkareem, Anti-wear properties evaluation of frictional sliding interfaces in automobile engines lubricated by copper/graphene nanolubricants, Friction 8 (5) (2020) 905–916, https://doi.org/10.1007/s40544-019-0308-0.
[52] X. Ran, X. Yu, Q. Zou, Effect of particle concentration on tribological properties of ZnO nanofluids, Tribology Transactions 60 (2017) 154–158, https://doi.org/10.1080/10402004.2016.1154233.